Algorithms to invert modern noble gas anomalies for the history of sea level pressure

Geoffrey Gebbie[1*]

[1]Department of Physical Oceanography, Woods Hole Oceanographic Institution,
360 Woods Hole Rd., Woods Hole, MA 02543, USA
[*]To whom correspondence should be addressed; E-mail: ggebbie@whoi.edu.

1 Overview

This text provides supporting information regarding numerical methods to invert modern oceanic noble gas anomalies for a timeseries of sea level pressure.

1.1 Ocean circulation links between temporal and spatial variability

Ocean tracers, including noble gas concentrations, carry the imprint of surface conditions into the subsurface ocean, making a record of past surface conditions in today's ocean. Surface conditions are transported to some parts of the subsurface ocean faster than others, and therefore past temporal variability leads to spatial variability in any snapshot of the ocean. Even globally-uniform changes at the surface will lead to subsurface gradients through this mechanism (*1, 2*).

We observe a noble gas difference between $35°$N and $10°$S along the meridional section at $150°$W and 3.5 km depth. This difference is isolated to a $p_\star = 2.8 \pm 0.4$ mbar sea level pressure difference during the formation of the waters, where $p_\star$ is the influence of pressure at the time that water leaves the surface mixed layer which is conservative in the subsurface. We suggest

the notation $p_\star$ or "preformed pressure" in analogy with $\mathrm{P}_\star$, the preformed phosphate (*3*). If these two locations have waters with sufficiently different ages, or elapsed time since water was last at the surface, the difference could be explained by the timing of past surface changes.

Here we calculate the age distributions for representative abyssal North and South Pacific sites from an empirically-derived steady-state ocean circulation model that fits modern-day climatological distributions of temperature, salinity, phosphate, nitrate, oxygen, oxygen-isotope ratio, and radiocarbon (*4*). Both sites have waters with a wide range of ages from a few hundred to a few thousand years (Figure 1) because of the many routes from abyssal water formation sites and the significant time for mixing to occur (*5*). The age distributions are peaked at about 800 and 1000 years for the South and North Pacific sites, respectively, indicating that the South Pacific has waters of a younger age due to being closer to Antarctic sites of abyssal water formation. Although abyssal Pacific waters move slowly and remain in the basin for a long time, there are clear meridional differences in the ages of seawater.

The preformed pressure value today (i.e., 2023 CE) at the North Pacific sample location r_{np} is related to the past via a convolution equation,

$$p_\star(2023\ \mathrm{CE}, r_{np}) = \sum_{i=1}^{3000} g_i(r_{np})\ p_\star(2023\ \mathrm{CE} - i\ \mathrm{yr}, r_b), \tag{1}$$

which is a sum of contributions from g_i, the annually-resolved age distribution, operating on the past surface boundary conditions at r_b (*6*). The distribution is denoted g_i to recall the discrete-time Green's function, and is available from the steady-state circulation for the past 4,000 years. The sum of g_i values is greater than 0.99 indicating that 4,000 years is sufficient to capture over 99% of the age distribution. Note that g_i is dimensionless and has been translated into a mass fraction per year to be displayed in continuous, rather than discrete, form in Figure 1. A similar equation is available for the South Pacific location.

The difference between the North and South Pacific age distributions is key for mapping

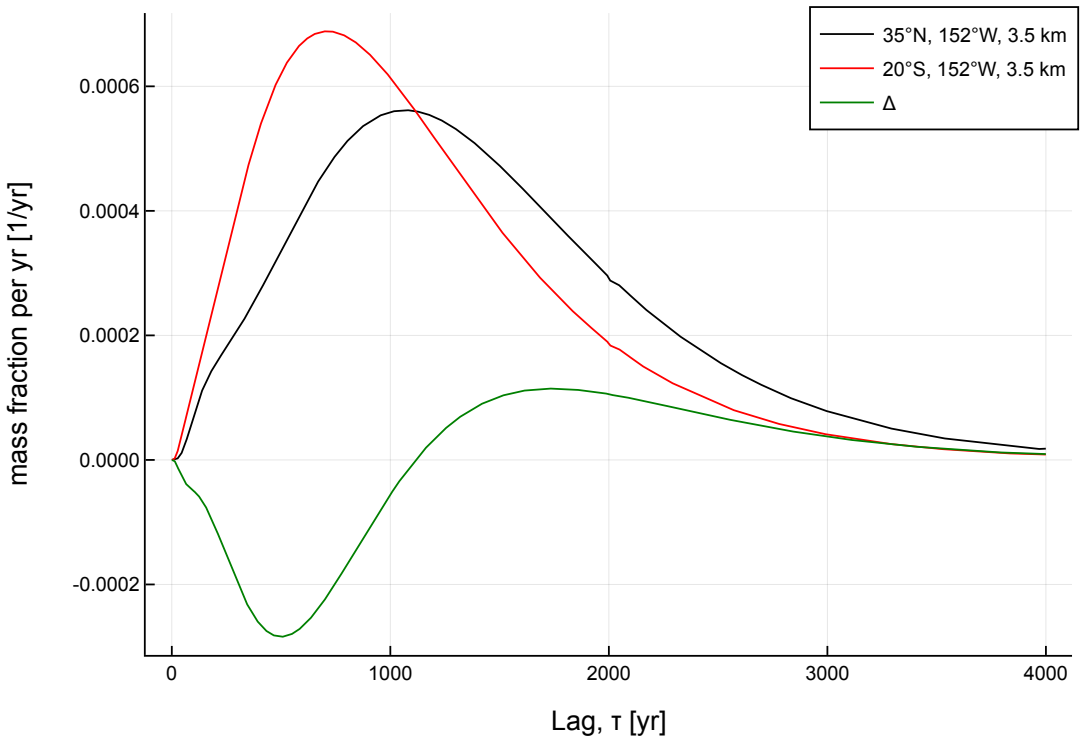

Figure 1. Age distributions from the North (*black*) and South (*red*) Pacific along $152°W$ and 3.5 km depth, as well as the north minus south difference (*green*), as calculated from an empirically-derived ocean circulation model. The integral under the black and red curves is such that the total mass fraction is unity. Lags on the x-axis refer to the time lag of subsurface signals relative to the surface.

time variability into space. The difference between equation (1) and an equivalent South Pacific equation yields a constraint on the preformed pressure difference:

$$\Delta p_\star(2023\ \mathrm{CE}, r_{np}, r_{sp}) = \sum_{i=1}^{4000} \Delta g_i\ p_\star(2023\ \mathrm{CE} - i\ \mathrm{yr}, r_b), \tag{2}$$

where $\Delta p_\star$ is the north minus south preformed pressure difference and the new Green's function is a difference (i.e., $\Delta g_i = g_i(r_{np}) - g_i(r_{sp})$ where r_{sp} refers to the South Pacific location. This equation is simplified under the assumption that the Green's functions are unchanging in time, an assumption that appears to be true to first order given the slight modifications to ocean hydrographic structure over the past 150 years (*2*). It is also assumed that past changes in preformed phosphate are globally-uniform, which is clearly untrue and will be interpreted later in this document. In concept, equation (4) relates a spatial gradient on the left hand side to a surface timeseries on the right hand side.

The north-south difference in age distributions shows negative values around 500 years and positive values around 1,500 years (green, Figure 1), as is possible because differences of distributions are no longer required to be non-negative. If surface conditions imprinted the signal of higher pressure 500 years ago, it would be reflected with South Pacific preformed pressure being higher than the North Pacific. What is actually observed is the North Pacific being higher than the South, suggesting that surface conditions had lower pressure 500 years ago. Any timeseries of surface changes that projects on Δg_i, however, also affect today's meridional gradient in $p_\star$, and a quantitative method is required to sort through the range of plausible solutions.

Another concern is whether ocean mixing would erase the signal of past surface conditions before they could be recorded today. The magnitude and shape of the curve that represents Δg_i in Figure 1 contains information about this mixing and damping of surface signals through time. In some sense, Δg_i is analogous to an ocean circulation filter which acts to transform the surface timeseries. Thus, any quantitative method must be able to perform a de-convolution to deter-

mine whether north-south age differences are large enough to explain the observed preformed-pressure spatial gradient.

1.2 Seawater vintages

It is highly unlikely that noble gases contain information about year-to-year to even decade-to-decade changes. Therefore, we simplify the analysis by defining vintages of seawater that describe the epoch during which water was last at the surface. Vintages have previously been used to describe the year that waters left the surface (*7*), like a vintner describes a batch of wine, and here we use the term for a much wider range of years. Here we define the following vintages: modern (MOD, 1800 - 2022 CE), Little Ice Age (LIA, 1300- 1800 CE), Medieval Climate Anomaly (MCA, 800 - 1300), Dark Ages Cold Period (DACP, 300 -800 CE), Roman Warm Period (RWP, 200 BCE - 300 CE), and the pre-Roman Warm Period (preRWP, before 200 BCE). Note that these time intervals do not strictly match definitions in the literature (*8*), but instead are chosen to prioritize 500-year intervals for ease of later interpretation.

The description of the waters that bathe the North and South Pacific sites can now be simplified to the combination of these six vintages. The mass fraction of each vintage is calculated by integrating the age distribution over the appropriate time interval, for example for the Little Ice Age (LIA),

$$m_{LIA}(r_{np}) = \sum_{i=2023-1800}^{2023-1300} g_i(r_{np}), \tag{3}$$

where m_{LIA} is the mass fraction of LIA water and the time indices account for the time elapsed between the LIA and today. Following the development above, the key relationship between temporal and spatial gradients is simplied,

$$\Delta p_\star(2023\ \mathrm{CE}, r_{np}, r_{sp}) = \sum_{j=1}^{6} \Delta m_j\ p_\star(j, r_b), \tag{4}$$

where the summation include six vintages, the mass-fraction difference is $\Delta m_j = m_j(r_{np}) -$

$m_j(r_{sp})$, and the history of surface boundary conditions is identified with a particular climate epoch. This simplification makes a tradeoff; it will be more difficult to explain the observations but all solutions will represent a realistic system with centennial-scale changes in climate.

1.3 Inverse problem

Equation (4) represents an underdetermined problem with one constraint, six unknowns, and infintely-many solutions. Here we provide information regarding the expected covariance of the solution to construct a statistical solution with its uncertainty. The solution method, detailed next, is based on the Gauss-Markov Theorem (*9*).

For ease of notation we collate the unknown parameters and the vintage mass fractions into vectors:

$$\mathbf{x} = \begin{pmatrix} p_\star(\mathrm{MOD}, r_b) \\ p_\star(\mathrm{LIA}, r_b) \\ p_\star(\mathrm{MCA}, r_b) \\ p_\star(\mathrm{DACP}, r_b) \\ p_\star(\mathrm{RWP}, r_b) \\ p_\star(\mathrm{preRWP}, r_b) \end{pmatrix}, \tag{5}$$

and

$$\mathbf{m} = \begin{pmatrix} \Delta m_{MOD} \\ \Delta m_{LIA} \\ \Delta m_{MCA} \\ \Delta m_{DACP} \\ \Delta m_{RWP} \\ \Delta m_{preRWP} \end{pmatrix}. \tag{6}$$

Now the constraint is symbolically described as,

$$y = \mathbf{m}^T \mathbf{x} + \mathbf{n}, \tag{7}$$

where the observation is $y = \Delta p_\star(2023\ \mathrm{CE}, r_{np}, r_{sp})$, T is the vector transpose, and $\mathbf{n}$ is a reminder that the observational fit is not expected to be perfect.

The Gauss-Markov Theorem provides a means to solve an underdetermined problem via the

solution formula,

$$\tilde{\mathbf{x}} = \mathbf{C}_{xx}\mathbf{m}(\mathbf{m}^T\mathbf{C}_{xx}\mathbf{m} + \mathbf{C}_{nn})^{-1}y \tag{8}$$

which is valid so long as the quantity in parentheses is invertible. We denote $\tilde{\mathbf{x}}$ with a tilde to mark that it is a solution. The observation y is not bold because it is a scalar, not a vector. This solution satisfies a number of advantageous statistical properties, such as being unbiased and minimizing the uncertainty of each solution element. Such properties only hold in the case that the input statistical information, the solution and observation covariance matrices $\mathbf{C}_{xx}$ and C_{nn} are valid.

The observational covariance is easily set as it is the observational variance: $C_{nn} = (0.4\text{mbar})^2$. The solution covariance has two components: 1) setting the baseline or reference for the pre-formed pressure anomalies, and 2) a description of the expected climate variability. Here we define the reference for the anomalies to be the pre-industrial (all vintages but MOD) $p_\star$ average. Such a constraint could be added to the system as a second observational equation of the form:

$$\bar{p_\star} = \sum_{j=2}^{6} \frac{1}{5} p_\star(j, r_b) = \overline{\mathbf{m}}^T\mathbf{x} = 0, \tag{9}$$

where $(1/5)$ arises from the average over five vintages. Instead we recognize that this constraint imposes a covariance of the form, $\mathbf{C}_{xx} = \sigma^2\overline{\mathbf{m}}^T\overline{\mathbf{m}}$, where σ is the expected deviation from a perfect zero reference level. Here we choose the small but non-zero value of $\sigma = 10^{-4}$ mbar.

For part (2) of the solution covariance, we experiment with three cases with increasing complexity.

- Minimum variance of solution

  We define the solution covariance to conservatively assume that $p_\star$ has a standard deviation of 10 mbar based upon existing sea level pressure gradients and historical model simulations (*10*). All epochs are assumed to vary independently. The solution covariance

is

$$\mathbf{C}_{xx} = \begin{pmatrix} 100.0 & 0.0 & 0.0 & 0.0 & 0.0 & 0.0 \\ 0.0 & 100.0 & 0.0 & 0.0 & 0.0 & 0.0 \\ 0.0 & 0.0 & 100.0 & 0.0 & 0.0 & 0.0 \\ 0.0 & 0.0 & 0.0 & 100.0 & 0.0 & 0.0 \\ 0.0 & 0.0 & 0.0 & 0.0 & 100.0 & 0.0 \\ 0.0 & 0.0 & 0.0 & 0.0 & 0.0 & 100.0 \end{pmatrix} \mathrm{mbar}^2 \tag{10}$$

The solution covariance from (1) that defines the anomaly reference level is added to this matrix, as is done in all cases to follow.

- Minimum trend

  The climate epochs are several hundred years long but the climate is known to have variability at these scales and longer. In this second case, we define the solution covariance such that trends have an expected magnitude no larger than $p\prime = 4$ mbar/century based upon the few long timescale climate frequency spectra that are available (*11*). We define a matrix $\mathbf{D}$ that calculates differences between all combinations of vintages, and where the expected output for vintages i and j is:

$$\Delta p_\star(i,j) = p\prime \Delta t(i,j) \tag{11}$$

  where $\Delta t(i,j)$ is the time difference between the midpoints of vintages i and j. The resulting covariance matrix is $\mathbf{D}\mathbf{D}^T$ where each element is scaled by $(1/\Delta p_\star(i,j))^2$.

- Combined covariance matrix

  The combined covariance matrix (labeled "min-trend-variance") is a sum of the covariance from (1) the definition of the reference level for preformed pressure anomalies, 2) the expected variance of preformed pressure about this reference level ("min-variance"), and 3) expectation of correlation between vintages that are adjacent in time ("min-trend").

1.4 Inverse solutions

The three inverse solutions use a variety of statistical input from different information sources but converge to a common solution between the Little Ice Age and Roman Warm Period (2,000 and 500 years ago (Figure 2). This time period is marked by a statistically-significant ($p = 0.05$) inferred decrease of sea level pressure by 17 ± 8 mbar. The solutions also have common elements prior to 1,500 years ago. The greatest differences come in relation to LIA to modern changes. Because seawater in the abyssal North Pacific has very little modern vintage water, we are unable to conclusively place modern sea level pressure in context of previous changes. It is possible that modern sea level pressure is about the same as the LIA, or it could be as much as 15 mbar higher.

The problem formulation has proceeded by assuming that sea level pressure changes are globally-uniform, but such large changes in sea level pressure would indicate a change in the mass of the atmosphere. The low solubility of nitrogen and oxygen in seawater make such large mass changes unlikely. Instead, the results of the inverse solution should be interpreted in a more nuanced way. Signals in abyssal waters primarily reflect surface signals at the sites of formation in polar oceans, and we lack direct information about the tropics and subtropics here. Thus, inferred changes in the LIA and earlier should be interpreted as changes in polar oceans, and constraints on the global mass of the atmosphere can be balanced by opposing changes in the tropics.

It is still debated whether the LIA is a North Atlantic-centric or global phenomenon. Our inferences of sea level pressure change are best interpreted as changes in polar regions and cannot directly be pinpointed as northern or southern hemisphere variability. Due to the water-mass composition of the abyssal Pacific being dominated by southern source waters, however, we suggest that the noble gas signal is more easily explained by changes in and around Antarctica. North Atlantic waters occupy less than half the mass of Antarctic waters in the abyssal North

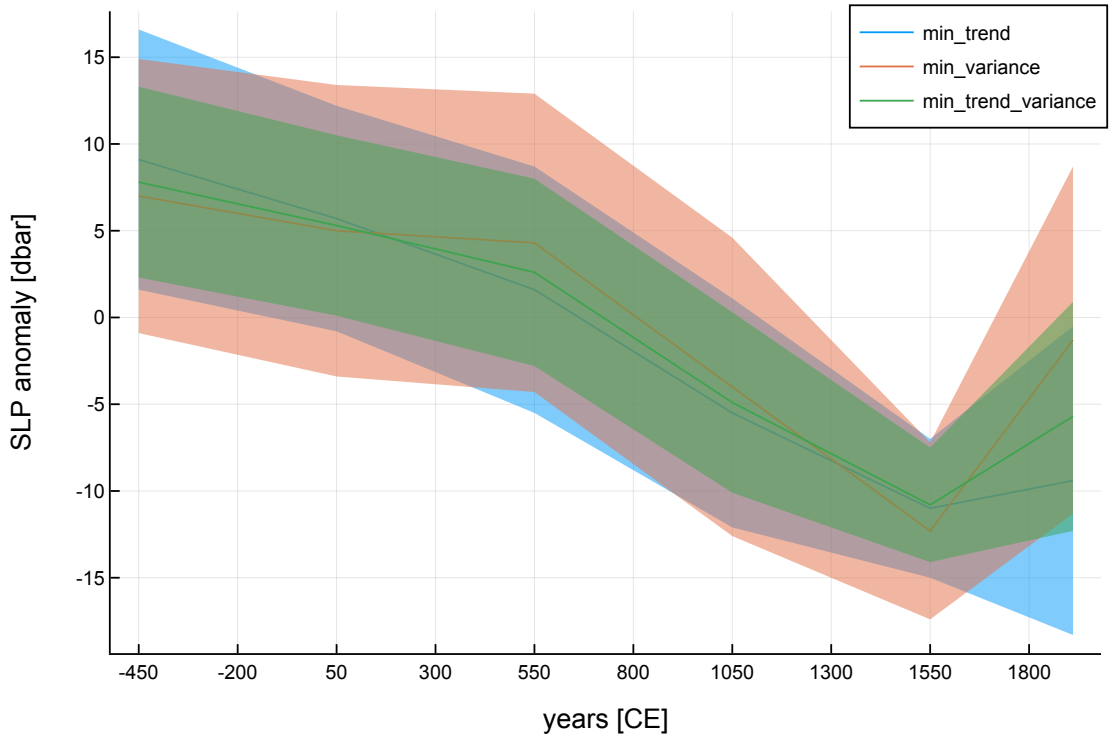

Figure 2. Inferred historical sea level pressure variations. All results use the identical noble gas observational information, but differ in the assumed solution covariance matrix (blue: min-trend, red: min-variance, green: min-trend-variance). Error ribbons represent the 1σ uncertainty level. Results from each vintage are plotted as a single value at the midpoint of the interval.

Table 1: Sea-level pressure differences in millibars between climate eras, as defined by the difference of the value during one vintage (*rows*) and another vintage (*columns*) calculated in the min-trend-variance case. Some differences are significant at the 67% (**bold**) and 95% (**bold, red**) confidence levels. The vintages are: modern (MOD, 1800 - 2022 CE), Little Ice Age (LIA, 1300- 1800 CE), Medieval Climate Anomaly (MCA, 800 - 1300), Dark Ages Cold Period (DACP, 300 -800 CE), Roman Warm Period (RWP, 200 BCE - 300 CE), and the pre-Roman Warm Period (preRWP, before 200 BCE).

Vintage	MOD	LIA	MCA	DACP	RWP	pre-RWP
MOD	0.0 ± 0.0	5.1 ± 7.2	-0.78 ± 8.9	-8.3 ± 8.6	**-10.9 ± 8.3**	**-13.5 ± 8.2**
LIA	-5.1 ± 7.2	0.0 ± 0.0	-5.8 ± 7.9	**-13.4 ± 6.7**	**-16.0 ± 6.1**	**-18.5 ± 5.6**
MCA	0.8 ± 8.9	5.8 ± 7.9	0.0 ± 0.0	-7.5 ± 7.8	**-10.2 ± 8.1**	**-12.7 ± 8.3**
DACP	8.3 ± 8.6	**13.4 ± 6.7**	7.5 ± 7.8	0.0 ± 0.0	-2.6 ± 8.5	-5.1 ± 9.5
RWP	**10.9 ± 8.3**	**16.0 ± 6.1**	**10.2 ± 8.1**	2.6 ± 8.5	0.0 ± 0.0	-2.5 ± 9.0
pre-RWP	**13.5 ± 8.2**	**18.5 ± 5.6**	**12.7 ± 8.3**	5.1 ± 9.5	2.5 ± 9.0	0.0 ± 0.0

Pacific (*12*), and would require an sea level pressure signal that is more than twice as large (30+ mbar) if the Antarctic region did not participate in the LIA.

1.5 Sea-level pressure differences between climate eras

The scenario with the highest degree of sophistication is labeled "min-trend-variance." The long-term trend between the Little Ice Age and the earliest climate eras (Dark Ages Cold Period, Roman Warm Period, and pre-Roman Warm Period) is significant at the 95% confidence level (Table 1.5). In particular, we estimate that the pre-RWP to LIA decrease of 19 ± 11 mbar (2σ error bars) is well constrained by the data. Differences over shorter time periods are generally not significant. It is also difficult to find a significant relation to modern sea level pressures.